Journal of Sound and Vibration 329 (2010) 5017–5035

Contents lists available at ScienceDirect

Journal of Sound and Vibration

journal homepage: www.elsevier.com/locate/jsvi

Partial pole placement in structures by the method of receptances: Theory and experiments

Maryam Ghandchi Tehrani, Robin N.R. Elliott, John E. Mottershead *

Department of Engineering, University of Liverpool, Liverpool L69 3GH, UK

ARTICLE INFO

Article history:
Received 26 January 2010
Received in revised form
18 June 2010
Accepted 21 June 2010
Handling Editor: J. Lam

ABSTRACT

The theory and practical application of the receptance method for vibration suppression in structures by multi-input partial pole placement is described. Numerous advantages of the receptance method over conventional matrix methods such as state-space control based on finite elements have been demonstrated, in particular there is no need to know or to evaluate the structural matrices **M**, **C**, **K** and in practical experimentation the measurement of 'receptance' may be generalised so that explicit modelling of actuator dynamics becomes unnecessary. Active vibration control is demonstrated experimentally using two test rigs. In the first set of experiments partial pole placement is applied to a lightweight glass-fibre beam using macro fibre composite (MFC) actuators and sensors. In the second set of experiments active vibration control is implemented on a heavy modular test structure representative of systems of differing dynamic complexity using electromagnetic actuators and piezoelectric (ICP) accelerometers. It is demonstrated that chosen poles may be assigned to predetermined values without affecting the position of other poles of interest.

1. Introduction

The problem of pole placement has received considerable attention from the active-control and vibrations communities over several decades [1]. Applications where it is desirable to set natural frequencies and damping to specified values include the avoidance of damaging large-amplitude vibrations close to resonance, and the design of adaptive structures, capable of changing their behaviour to respond in a desirable way to a varying demand. Eigenvalue assignment in active-control dates from the 1960s when Wonham [2] showed that the poles of a system could be assigned by state feedback if the system was controllable. Porter and Crossley [3] developed a modal control method for systems described using the first-order state-space. Chu and Datta [4] addressed the problem of robust eigenvalue assignment in second-order systems, such as damped vibrating structures.

Del Vescovo and D'Ambrogio [5] described a receptance-based method for active vibration control and Ram and Mottershead [6] presented a new and general formulation for pole-zero placement in structures also using measured receptances. This approach has significant advantages over methods based upon finite element models, which are typically very large and easily degraded by model reduction. Finite element models also have difficulty in accurately modelling damping, which is critical to complex eigenvalue analysis. The receptance method does not require evaluation or knowledge of the system matrices **M**, **C**, **K**, and in principle, a single input may be used to assign all the poles of the system—when the poles are controllable. Conventional methods involve a tacit assumption that the dimension of the system is finite and measurable at every coordinate. The resulting set of state equations is only complete when all the displacements are available. However, when using the receptance method the system equations are inverted. This means

* Corresponding author.
E-mail address: j.e.mottershead@liv.ac.uk (J.E. Mottershead).

0022-460X/$ - see front matter © 2010 Elsevier Ltd. All rights reserved.
doi:10.1016/j.jsv.2010.06.018

that the equations are complete for each measured displacement when the control forces are known. Generally these forces are measured and small in number. There is no need to estimate the unmeasured state using an observer or a Kalman filter and no need for model reduction. The **M**,**C**,**K** matrices generally include modelling inaccuracies and discretisation errors, which become increasingly significant at higher frequencies. Receptances, however, may be measured with good accuracy over the entire range of frequencies of interest without loss of accuracy of the vibration modes.

In the partial pole placement problem a subset of poles of a structure are set to specified values, while leaving the other poles of interest unchanged. The problem was considered in the single-input case by Datta et al. [7], and in the multi-input case by Datta and Sarkissian [8]. Qian and Xu [9], Brahma and Datta [10] and Bai et al. [11] described various numerical routines for minimising the condition number of the matrix of closed-loop eigenvectors, for robust partial pole placement. However, these partial pole placement studies assume the system matrices are known (or estimated from methods such as finite elements). The use of the receptance method for robust multi-input pole placement is derived by Tehrani et al. [12], for the case where the system matrices are not known (nor required to be estimated).

Mottershead et al. [13] formulated a multiple-input–multiple-output (MIMO) approach by output-feedback control using collocated actuators and sensors and completed the first experimental pole-zero placement tests by the receptance method on a 'T' shaped thin plate, using small inertial actuators. The use of collocated actuators and sensors is helpful in overcoming the spillover problem since it is a configuration that closely mimics a passive modification, when time delays are negligible. Of course a structure cannot be destabilised by a passive modification since the system matrices maintain their symmetry and definiteness properties. Unfortunately, there are numerous examples of systems where collocation of actuators and sensors is impractical or impossible, usually because of inaccessible actuator locations. The multiple-input state feedback method proposed and applied in this paper is applicable to the most general case of non-collocated sensors and actuators. The use of the method to assign a subset of the poles of a system is demonstrated numerically, and in two set of experimental tests on (i) a lightweight composite beam with macro fibre composite actuators and sensors and (ii) a modular test structure in two configurations using electromagnetic actuators and piezoelectric (ICP) accelerometers. Another advantage of the method is revealed in the experiments, where the receptance is generalised to the transfer function between outputs and inputs of any measurable quantities (not necessarily displacement outputs and force inputs). In this way actuator dynamics may be included in the measured 'receptance' and do not need to be modelled, as for example in Xing et al. [14]. In contrast to the study by Datta et al. [7], which relies on ensuring modes not to be altered are unobservable, in this work these modes are rendered uncontrollable.

2. Preliminary calculations

In conventional modelling the dynamic behaviour of a structure is determined from mass, damping and stiffness matrices, $\mathbf{M}$, $\mathbf{C}$, $\mathbf{K} \in \Re^{n\times n}$, usually obtained from finite elements and with the usual symmetry and definiteness properties. In theory the receptance matrix, which is measurable experimentally, is the inverse of the dynamic stiffness matrix,

$$\mathbf{H}(s) = \mathbf{Z}^{-1}(s) \tag{1}$$

$$\mathbf{Z}(s) = \mathbf{M}s^2 + \mathbf{C}s + \mathbf{K} \tag{2}$$

Orthogonality conditions for the quadratic pencil (2) were given by Fawzy and Bishop [15] and also by Datta et al. [7],

$$\left.\begin{array}{l} \boldsymbol{\varphi}_k^{\mathrm{T}}[(\lambda_j+\lambda_k)\mathbf{M}+\mathbf{C}]\boldsymbol{\varphi}_j = 0 \\ \boldsymbol{\varphi}_k^{\mathrm{T}}[\lambda_j\lambda_k\mathbf{M}-\mathbf{K}]\boldsymbol{\varphi}_j = 0 \end{array}\right\}, \quad j \neq k \tag{3}$$

$$\begin{aligned} \boldsymbol{\varphi}_k^{\mathrm{T}}[2\lambda_k\mathbf{M}+\mathbf{C}]\boldsymbol{\varphi}_k &= 1 \\ \boldsymbol{\varphi}_k^{\mathrm{T}}[\lambda_k^2\mathbf{M}-\mathbf{K}]\boldsymbol{\varphi}_k &= \lambda_k \end{aligned} \tag{4}$$

where $\lambda_k \in \{\lambda_j, \lambda_j^*\}_{j=1}^n$ denote the eigenvalues and $\boldsymbol{\varphi}_k \in \{\boldsymbol{\varphi}_j, \boldsymbol{\varphi}_j^*\}_{j=1}^n$ are the eigenvectors of the system. The receptance matrix, $\mathbf{H}(s)$, may be expressed in terms of the eigenvalues and eigenvectors of the system,

$$\mathbf{H}(s) = \sum_{k=1}^{n} \left(\frac{\boldsymbol{\varphi}_k \boldsymbol{\varphi}_k^{\mathrm{T}}}{(s-\lambda_k)} + \frac{\boldsymbol{\varphi}_k^* \boldsymbol{\varphi}_k^{*\mathrm{T}}}{(s-\lambda_k^*)} \right) \tag{5}$$

or by the ratio of two polynomials,

$$\mathbf{H}(s) = \frac{\mathbf{N}(s)}{d(s)} \tag{6}$$

where $d(\lambda_k)=0$ is the characteristic equation that defines the eigenvalues of the system. The polynomial $d(s)$ and the matrix $\mathbf{N}(s)$ may be expanded as

$$d(s)=\prod_{k=1}^{n}((s-\lambda_k)(s-\lambda_k^*)) \tag{7}$$

and

$$\mathbf{N}(s)=\begin{bmatrix}\boldsymbol{\Phi} & \boldsymbol{\Phi}^*\end{bmatrix}\ \mathrm{adj}\begin{pmatrix}\mathrm{diag}(s-\lambda_k) & \mathbf{0}\\ \mathbf{0} & \mathrm{diag}(s-\lambda_k^*)\end{pmatrix}\ \begin{bmatrix}\boldsymbol{\Phi} & \boldsymbol{\Phi}^*\end{bmatrix}^{\mathrm{T}} \tag{8}$$

where $\boldsymbol{\Phi}$ is the modal matrix of mass-normalised eigenvector columns,

$$\begin{bmatrix}\boldsymbol{\Phi} & \boldsymbol{\Phi}^*\end{bmatrix}=\begin{bmatrix}\boldsymbol{\varphi}_1 & \cdots & \boldsymbol{\varphi}_n & \boldsymbol{\varphi}_1^* & \cdots & \boldsymbol{\varphi}_n^*\end{bmatrix} \tag{9}$$

It follows from Eq. (8) that $\mathrm{rank}(\mathbf{N}(s))=1$ if and only if $s=\lambda_k$,

$$\mathbf{N}(\lambda_j)=\boldsymbol{\varphi}_k\left(\prod_{\substack{j=1\\ j\neq k}}^{n}(\lambda_k-\lambda_j)\prod_{j=1}^{n}(\lambda_k-\lambda_j^*)\right)\boldsymbol{\varphi}_k^{\mathrm{T}} \tag{10}$$

The dynamic stiffness equation,

$$\mathbf{Z}(s)\mathbf{x}(s)=\mathbf{f}(s) \tag{11}$$

is a 'force' equation. Every term in $\mathbf{x}(s)$, the displacement or state vector, must be present for the equation to be complete. This is the reason why, in state-space control problems, it is necessary to use an observer (or equivalent) to estimate the unmeasured states. In industrial-scale problems the number of coordinates can be many thousands, or even millions, and therefore it is necessary to use model reduction methods to condense the problem to an acceptable size. On the other hand, the receptance equation, expressed as

$$\mathbf{H}(s)\mathbf{f}(s)=\mathbf{x}(s) \tag{12}$$

is a 'displacement' equation. For each row of the matrix equation to be complete it is only necessary to know the applied forces, usually at a small number of coordinates. Therefore for every sensor location, the measured terms in $\mathbf{x}(s)$, one only needs to know the non-zero terms in $\mathbf{f}(s)$, which are usually measured in an experiment. Therefore, there is no requirement for an observer or for model reduction when using the receptance method.

In practical problems we may be interested to modify the spectrum (the natural frequencies and damping ratios) of a system, usually to avoid resonances with excitation frequencies. This may be achieved by modifying the system, either passively by adding mass, damping or stiffness terms, or by active control. The advantage of passive modification is that the modified system is guaranteed to remain stable. However, practical modification requires difficult measurements, typically rotational receptances [16]. The advantage of active control is that it offers much greater freedom in the 'form' of the modification, but this is achieved at the expense of 'compensation' to ensure stability. The simplest modification is the unit-rank dynamic-stiffness modification,

$$\overline{\mathbf{Z}}(s)=\mathbf{Z}(s)+\mathbf{u}(s)\mathbf{v}^{\mathrm{T}}(s) \tag{13}$$

and a straightforward solution is available for the modified receptance matrix by the Sherman–Morrison formula [17];

$$\overline{\mathbf{H}}(s)=\mathbf{H}(s)-\frac{\mathbf{H}(s)\mathbf{u}(s)\mathbf{v}^{\mathrm{T}}(s)\mathbf{H}(s)}{1+\mathbf{v}^{\mathrm{T}}(s)\mathbf{H}(s)\mathbf{u}(s)} \tag{14}$$

where $\overline{\mathbf{Z}}(s)$ and $\overline{\mathbf{H}}(s)$ are, respectively, the dynamic stiffness and receptance matrices of the modified system. The characteristic equation is

$$1+\mathbf{v}^{\mathrm{T}}(\mu_k)\mathbf{H}(\mu_k)\mathbf{u}(\mu_k)=0 \tag{15}$$

where $\{\mu_k\}_{k=1}^{2n}$ are the eigenvalues of the modified system. Such characteristic equations form the basis of the method of receptances. This approach, fully explained in [6] and restricted to the assignment of simple eigenvalues, is extended in the present article.

3. Modal controllability and observability

The controllability and observability of vibration modes were considered by Hamdan and Nayfeh [18]. For the case of a second-order system with single input, $u(s)$, and output, $y(s)$, they wrote,

$$(\mathbf{M}s^2+\mathbf{C}s+\mathbf{K})\mathbf{x}(s)=\mathbf{b}u(s) \tag{16}$$

$$y(s)=-\begin{pmatrix}\mathbf{f}^{\mathrm{T}} & \mathbf{g}^{\mathrm{T}}\end{pmatrix}\begin{pmatrix}s\mathbf{x}\\ \mathbf{x}\end{pmatrix}=-(s\mathbf{f}+\mathbf{g})^{\mathrm{T}}\mathbf{x} \tag{17}$$

and showed that the kth mode is (i) controllable if and only if

$$\operatorname{rank}\left[\lambda_k^2\mathbf{M}+\lambda_k\mathbf{C}+\mathbf{K} \quad \vdots \quad \mathbf{b}\right]=n \tag{18}$$

and (ii) observable if and only if

$$\operatorname{rank}\begin{bmatrix}\mathbf{g}^{\mathrm{T}}+\lambda_k\mathbf{f}^{\mathrm{T}}\\ \lambda_k^2\mathbf{M}+\lambda_k\mathbf{C}+\mathbf{K}\end{bmatrix}=n \tag{19}$$

They defined measures of modal controllability and observability as the cosines of angles between one-dimensional subspaces,

$$\cos\theta_{(c)k}=\left(\frac{|\boldsymbol{\varphi}_k^{\mathrm{T}}\mathbf{b}|}{\|\boldsymbol{\varphi}_k\|\|\mathbf{b}\|}\right),\quad \cos\theta_{(o)k}=\left(\frac{|\boldsymbol{\varphi}_k^{\mathrm{T}}(\mathbf{g}+s\mathbf{f})|}{\|\boldsymbol{\varphi}_k\|\|\mathbf{g}+s\mathbf{f}\|}\right) \tag{20),(21}$$

where $\boldsymbol{\varphi}_k$ is the kth open-loop eigenvector.

The distance between the kth mode and the input distribution $\mathbf{b}$ becomes a maximum when $\boldsymbol{\varphi}_k^{\mathrm{T}}\mathbf{b}=0$ and the kth mode is then said to be *uncontrollable*. Likewise the kth mode is said to be *unobservable* when $\boldsymbol{\varphi}_k^{\mathrm{T}}(\mathbf{g}+s\mathbf{f})=0$.

We combine Eqs. (16) and (17) using $u(s)=y(s)$. Then,

$$(\mathbf{M}s^2+(\mathbf{C}+\mathbf{b}\mathbf{f}^{\mathrm{T}})s+(\mathbf{K}+\mathbf{b}\mathbf{g}^{\mathrm{T}}))\mathbf{x}(s)=0 \tag{22}$$

which amounts to a rank-1 modification to the dynamic stiffness matrix.

Now by setting $s=\lambda_k$ and premultiplying Eq. (22) by $\boldsymbol{\varphi}_k^{\mathrm{T}}$,

$$\boldsymbol{\varphi}_k^{\mathrm{T}}(\mathbf{M}\lambda_k^2+\mathbf{C}\lambda_k+\mathbf{K})\boldsymbol{\varphi}_k=-(\boldsymbol{\varphi}_k^{\mathrm{T}}\mathbf{b})((\mathbf{g}^{\mathrm{T}}+\lambda_k\mathbf{f}^{\mathrm{T}})\boldsymbol{\varphi}_k) \tag{23}$$

The right-hand side vanishes whenever $(\boldsymbol{\varphi}_k^{\mathrm{T}}\mathbf{b})=0$, the *uncontrollability* condition, or $(\mathbf{g}^{\mathrm{T}}+\lambda_k\mathbf{f}^{\mathrm{T}})\boldsymbol{\varphi}_k=0$, the *unobservability* condition. We notice that under either of these conditions the eigenvalue λ_k remains unchanged by control action. The eigenvectors $\boldsymbol{\varphi}_k$ in Eq. (23) do not have the effect of diagonalising $\mathbf{M}$, $\mathbf{C}$, $\mathbf{K}$ separately, but we see from the orthogonality conditions (3)–(4) that the dynamic stiffness $(\lambda_k^2\mathbf{M}+\lambda_k\mathbf{C}+\mathbf{K})$ is indeed diagonalised. In general Eq. (23) leads to the asymmetric quadratic eigenvalue problem:

$$(\mathbf{M}\mu_k^2+(\mathbf{C}+\mathbf{b}\mathbf{f}^{\mathrm{T}})\mu_k+(\mathbf{K}+\mathbf{b}\mathbf{g}^{\mathrm{T}}))\boldsymbol{\psi}_k=\mathbf{0} \tag{24}$$

where $\{\boldsymbol{\psi}_k\}_{k=1}^{2n}$ denote the closed-loop eigenvectors. We note that uncontrollability and unobservabilty are not the only conditions under which right-hand side of Eq. (23) will vanish, but they are the only ones that will be considered in the analysis and practical experiments that follow.

4. Partial pole placement

Datta et al. [7] developed a method for finding $\{\mathbf{f},\mathbf{g}\}$ such that a partial set of eigenvalues $\{\lambda_k,\lambda_k^*\}_{k=1}^{m}$ are assigned to a desired set $\{\mu_k,\mu_k^*\}_{k=1}^{m}$, while keeping all other eigenvalues unchanged $\{\mu_k=\lambda_k,\mu_k^*=\lambda_k^*\}_{k=m+1}^{n}$. The problem, termed *partial pole placement*, is to solve the two systems of characteristic equations:

$$\left.\begin{aligned}&\det(\mu_k^2\mathbf{M}+\mu_k(\mathbf{C}+\mathbf{b}\mathbf{f}^{\mathrm{T}})+\mathbf{K}+\mathbf{b}\mathbf{g}^{\mathrm{T}})=0\\ &\det(\mu_k^{*2}\mathbf{M}+\mu_k^*(\mathbf{C}+\mathbf{b}\mathbf{f}^{\mathrm{T}})+\mathbf{K}+\mathbf{b}\mathbf{g}^{\mathrm{T}})=0\end{aligned}\right\}_{k=1}^{m} \tag{25}$$

$$\left.\begin{aligned}&\det(\lambda_k^2\mathbf{M}+\lambda_k(\mathbf{C}+\mathbf{b}\mathbf{f}^{\mathrm{T}})+\mathbf{K}+\mathbf{b}\mathbf{g}^{\mathrm{T}})=0\\ &\det(\lambda_k^{*2}\mathbf{M}+\lambda_k^*(\mathbf{C}+\mathbf{b}\mathbf{f}^{\mathrm{T}})+\mathbf{K}+\mathbf{b}\mathbf{g}^{\mathrm{T}})=0\end{aligned}\right\}_{k=m+1}^{n} \tag{26}$$

They showed the following solution satisfied Eqs. (25) and (26), for arbitrary vector $\boldsymbol{\beta}=(\beta_1 \quad \beta_2 \quad \cdots \quad \beta_m)^{\mathrm{T}}$,

$$\mathbf{f}=-\mathbf{M}(\boldsymbol{\Phi}_1\boldsymbol{\Lambda}_1\boldsymbol{\beta}+\boldsymbol{\Phi}_1^*\boldsymbol{\Lambda}_1^*\boldsymbol{\beta}^*) \tag{27}$$

$$\mathbf{g}=\mathbf{K}(\boldsymbol{\Phi}_1\boldsymbol{\beta}+\boldsymbol{\Phi}_1^*\boldsymbol{\beta}^*) \tag{28}$$

where $\boldsymbol{\Phi}_1=\begin{bmatrix}\boldsymbol{\varphi}_1 & \boldsymbol{\varphi}_2 & \cdots & \boldsymbol{\varphi}_m\end{bmatrix}$ is the matrix composed of eigenvectors of the open-loop system (1) corresponding to the small number of the altered eigenvalues,

$$\boldsymbol{\Lambda}_1=\operatorname{diag}(\mu_k)_{k=1}^{m} \tag{29}$$

An explicit solution for $\boldsymbol{\beta}$ was given in the form:

$$\{\beta_k\}_{k=1}^{m} = \frac{1}{\mathbf{b}^{\mathrm{T}}\boldsymbol{\varphi}_k}\frac{\mu_k-\lambda_k}{\lambda_k}\prod_{\substack{r=1\\ r\neq k}}^{m}\frac{\mu_r-\lambda_k}{\lambda_r-\lambda_k}\Bigg|_{k=1}^{m} \tag{30}$$

4.1. Partial pole placement using the unobservability condition

From the unobservability condition, $(\mathbf{g}+\mu_k\mathbf{f})^{\mathrm{T}}\boldsymbol{\varphi}_k = 0$, and using Eqs. (27) and (28),

$$-(\boldsymbol{\beta}^{\mathrm{T}}\boldsymbol{\Lambda}_1\boldsymbol{\Phi}_1^{\mathrm{T}}+\boldsymbol{\beta}^{*\mathrm{T}}\boldsymbol{\Lambda}_1^{*}\boldsymbol{\Phi}_1^{*\mathrm{T}})\mathbf{M}\boldsymbol{\varphi}_k\lambda_k+(\boldsymbol{\beta}^{\mathrm{T}}\boldsymbol{\Phi}_1^{\mathrm{T}}+\boldsymbol{\beta}^{*\mathrm{T}}\boldsymbol{\Phi}_1^{*\mathrm{T}})\mathbf{K}\boldsymbol{\varphi}_k = 0 \tag{31}$$

Since

$$\lambda_k \in (\,\lambda_{m+1}\quad \lambda_{m+2}\quad \cdots\quad \lambda_n,\quad \lambda_{m+1}^{*}\quad \lambda_{m+2}^{*}\quad \cdots\quad \lambda_n^{*}\,) \tag{32}$$

and

$$\boldsymbol{\varphi}_k \in \begin{bmatrix}\boldsymbol{\Phi}_2 & \boldsymbol{\Phi}_2^{*}\end{bmatrix},\quad \boldsymbol{\Phi}_2 = \begin{bmatrix}\boldsymbol{\varphi}_{m+1} & \boldsymbol{\varphi}_{m+2} & \cdots & \boldsymbol{\varphi}_n\end{bmatrix} \tag{33}$$

it becomes clear from orthogonality, Eq. (3), that the terms $\boldsymbol{\Lambda}_1\boldsymbol{\Phi}_1^{\mathrm{T}}\mathbf{M}\boldsymbol{\varphi}_k\lambda_k+\boldsymbol{\Phi}_1^{\mathrm{T}}\mathbf{K}\boldsymbol{\varphi}_k$ and $\boldsymbol{\Lambda}_1^{*}\boldsymbol{\Phi}_1^{*\mathrm{T}}\mathbf{M}\boldsymbol{\varphi}_k\lambda_k+\boldsymbol{\Phi}_1^{*\mathrm{T}}\mathbf{K}\boldsymbol{\varphi}_k$ in Eq. (31) are both null vectors. The unobservability condition is fulfilled so that $\mu_k=\lambda_k$ remains unchanged irrespective of the choice of $\boldsymbol{\beta}$. Thus, Datta's method [7] is seen to work by causing the unchanged eigenvalues to be unobservable.

The use of the orthogonality condition implies that a sensor must be located at every degree of freedom of the system, which is impractical. It is not necessary for there to be an actuator at every degree of freedom. Also it is necessary to know **M** and **K**, which we would like to avoid when using a receptance-based approach. However, partial pole placement may be achieved by using the dual concepts of observability and controllability as will be explained in what follows, in other words we seek partial pole placement by applying a condition of uncontrollability.

4.2. Partial pole placement using the uncontrollability condition

The uncontrollability condition may be expressed as $\mathbf{b}^{\mathrm{T}}\boldsymbol{\varphi}_k = 0$, and if $\mathbf{b} \in \Re^n$ then there will be many cases when the condition cannot be met since **b** must be perpendicular to both the real and imaginary parts of $\boldsymbol{\varphi}_k$ ($\boldsymbol{\varphi}_k$ may be normalised to be very close to being real but this is not possible in general). Therefore we now write the vector **b** in the form:

$$\mathbf{b}(s) = \mathbf{b}_1 + \frac{\mathbf{b}_2}{s} \tag{34}$$

which is the case of integral force feedback [19]. Of course other forms of $\mathbf{b}(s)$ are possible. Then for the retained eigenvalues, $\mathbf{b}(s)$ is sought that satisfies the expression:

$$\begin{bmatrix}\boldsymbol{\Phi}_2^{\mathrm{T}} & \boldsymbol{\Lambda}_2^{-1}\boldsymbol{\Phi}_2^{\mathrm{T}}\end{bmatrix}\begin{pmatrix}\mathbf{b}_1\\ \mathbf{b}_2\end{pmatrix} = \mathbf{0} \tag{35}$$

or

$$\begin{pmatrix}\mathbf{b}_1\\ \mathbf{b}_2\end{pmatrix} = \mathbf{V}\boldsymbol{\alpha},\quad \mathbf{V} = \mathrm{null}\begin{bmatrix}\boldsymbol{\Phi}_2^{\mathrm{T}} & \boldsymbol{\Lambda}_2^{-1}\boldsymbol{\Phi}_2^{\mathrm{T}}\end{bmatrix} = \mathrm{null}\begin{bmatrix}\Re(\boldsymbol{\Phi}_2^{\mathrm{T}}) & \Re(\boldsymbol{\Lambda}_2^{-1}\boldsymbol{\Phi}_2^{\mathrm{T}})\\ \Im(\boldsymbol{\Phi}_2^{\mathrm{T}}) & \Im(\boldsymbol{\Lambda}_2^{-1}\boldsymbol{\Phi}_2^{\mathrm{T}})\end{bmatrix} \tag{36),(37}$$

where $\boldsymbol{\Lambda}_2 = \mathrm{diag}(\lambda_k)_{k=m+1}^{n}$ is the diagonal matrix of retained eigenvalues and $\dim\begin{bmatrix}\Re(\boldsymbol{\Phi}_2^{\mathrm{T}}) & \Re(\boldsymbol{\Lambda}_2^{-1}\boldsymbol{\Phi}_2^{\mathrm{T}})\\ \Im(\boldsymbol{\Phi}_2^{\mathrm{T}}) & \Im(\boldsymbol{\Lambda}_2^{-1}\boldsymbol{\Phi}_2^{\mathrm{T}})\end{bmatrix} = 2(n-m)\times 2n$.

The terms in $\boldsymbol{\alpha}$ are used to select the columns of **V** so that the eigenvalues $\{\lambda_k\}_{k=m+1}^{n},\{\lambda_k^{*}\}_{k=m+1}^{n}$ are uncontrollable.

In this way we see that the measured spectrum may be separated into assigned modes and retained modes to achieve partial pole placement without using the orthogonality conditions. This means that there is no need to know or to evaluate the system matrices **M**, **C**, **K**, which is entirely consistent with the approach described by Ram and Mottershead [6], based on measured receptances from vibration tests.

5. Numerical example—4 degree of freedom system

Consider the following 4 degree of freedom **M**, **C**, **K** system:

$$\mathbf{M}=\begin{bmatrix}3 & & & \\ & 10 & & \\ & & 20 & \\ & & & 12\end{bmatrix},\quad \mathbf{C}=\begin{bmatrix}2.3 & -1 & & \\ -1 & 2.2 & -1.2 & \\ & -1.2 & 2.7 & -1.5 \\ & & -1.5 & 1.5\end{bmatrix},\quad \mathbf{K}=\begin{bmatrix}40 & -30 & & \\ -30 & 60 & -30 & \\ & -30 & 90 & -30 \\ & & -30 & 30\end{bmatrix}$$

The open-loop poles are:

$$\lambda_{1,2}=-0.0108\pm 0.8736\mathrm{i}$$
$$\lambda_{3,4}=-0.0809\pm 1.6766\mathrm{i}$$
$$\lambda_{5,6}=-0.1336\pm 2.5280\mathrm{i}$$
$$\lambda_{7,8}=-0.3980\pm 4.0208\mathrm{i}$$

We wish to assign the first two pairs of poles while the remaining poles are unchanged,

$$\mu_{1,2}=-0.03\pm 1\mathrm{i}$$

$$\mu_{3,4}=-0.1\pm 2\mathrm{i}$$

The terms $\mathbf{b}_1$ and $\mathbf{b}_2$ are obtained from the null-space of the unassigned open-loop eigenvectors:

$$\begin{bmatrix}\boldsymbol{\varphi}_5^{\mathrm{T}} & \dfrac{\boldsymbol{\varphi}_5^{\mathrm{T}}}{\lambda_5} \\ \boldsymbol{\varphi}_7^{\mathrm{T}} & \dfrac{\boldsymbol{\varphi}_7^{\mathrm{T}}}{\lambda_7}\end{bmatrix}\begin{pmatrix}\mathbf{b}_1 \\ \mathbf{b}_2\end{pmatrix}=\mathbf{0}$$

where

$$\boldsymbol{\varphi}_5^{\mathrm{T}}=\begin{bmatrix}-0.0941-0.2578\mathrm{i} & -0.0829-0.1727\mathrm{i} & 0.1056+0.2807\mathrm{i} & -0.0738-0.1775\mathrm{i}\end{bmatrix}$$
$$\boldsymbol{\varphi}_7^{\mathrm{T}}=\begin{bmatrix}-0.0535+0.2107\mathrm{i} & 0.0220-0.0613\mathrm{i} & -0.0033+0.0077\mathrm{i} & 0.0006-0.0014\mathrm{i}\end{bmatrix}$$

In this case,

$$\begin{bmatrix}\boldsymbol{\varphi}_5^{\mathrm{T}} & \dfrac{\boldsymbol{\varphi}_5^{\mathrm{T}}}{\lambda_5} \\ \boldsymbol{\varphi}_7^{\mathrm{T}} & \dfrac{\boldsymbol{\varphi}_7^{\mathrm{T}}}{\lambda_7}\end{bmatrix}^{\mathrm{T}}=\begin{bmatrix}-0.0941-0.2578\mathrm{i} & -0.0535+0.2107\mathrm{i} \\ -0.0829-0.1727\mathrm{i} & 0.0220-0.0613\mathrm{i} \\ 0.1056+0.2807\mathrm{i} & -0.0033+0.0077\mathrm{i} \\ -0.0738-0.1775\mathrm{i} & 0.0006-0.0014\mathrm{i} \\ 0.1036-0.0318\mathrm{i} & -0.0506-0.0183\mathrm{i} \\ 0.0698-0.0291\mathrm{i} & 0.0146+0.0069\mathrm{i} \\ -0.1129+0.0358\mathrm{i} & -0.0018-0.0010\mathrm{i} \\ 0.0715-0.0254\mathrm{i} & 0.0003+0.0002\mathrm{i}\end{bmatrix}$$

and

$$\mathrm{null}\begin{pmatrix}\Re\begin{pmatrix}\boldsymbol{\varphi}_5^{\mathrm{T}} & \dfrac{\boldsymbol{\varphi}_5^{\mathrm{T}}}{\lambda_5} \\ \boldsymbol{\varphi}_7^{\mathrm{T}} & \dfrac{\boldsymbol{\varphi}_7^{\mathrm{T}}}{\lambda_7}\end{pmatrix} \\ \Im\begin{pmatrix}\boldsymbol{\varphi}_5^{\mathrm{T}} & \dfrac{\boldsymbol{\varphi}_5^{\mathrm{T}}}{\lambda_5} \\ \boldsymbol{\varphi}_7^{\mathrm{T}} & \dfrac{\boldsymbol{\varphi}_7^{\mathrm{T}}}{\lambda_7}\end{pmatrix}\end{pmatrix}=\begin{bmatrix}0.1996 & -0.0023 & -0.0649 & 0.0436 \\ 0.7146 & 0.0394 & -0.2611 & 0.1725 \\ 0.2723 & 0.3580 & -0.4771 & 0.3078 \\ -0.5712 & 0.5065 & -0.4113 & 0.2447 \\ 0.1143 & 0.1676 & 0.0730 & -0.0610 \\ 0.1512 & 0.6275 & 0.3787 & -0.2347 \\ 0.0898 & 0.3726 & 0.5493 & 0.2839 \\ -0.0719 & -0.2303 & 0.2834 & 0.8212\end{bmatrix}$$

We choose the first column so that

$$\mathbf{b}=\begin{pmatrix}0.1996 \\ 0.7146 \\ 0.2723 \\ -0.5712\end{pmatrix}+\frac{1}{s}\begin{pmatrix}0.1143 \\ 0.1512 \\ 0.0898 \\ -0.0719\end{pmatrix}$$

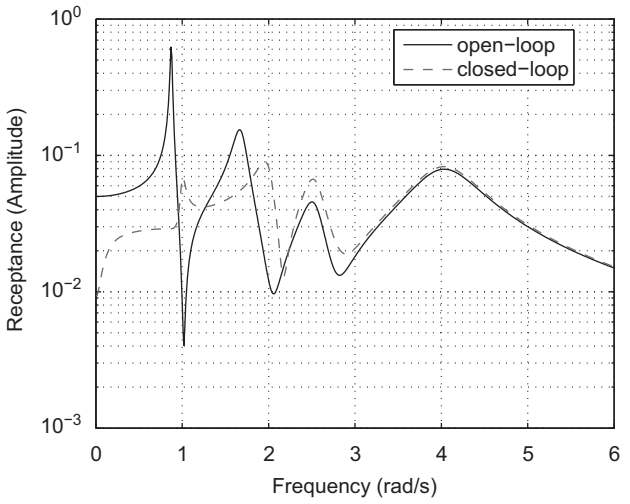

Fig. 1. Open-loop and closed-loop receptance for the 4 degree of freedom system.

Now we use single-input state feedback by the receptance method [6] to assign the poles using this **b**. The control gains are found to be

$$\mathbf{g}=\begin{pmatrix}10.1513\\12.1105\\8.1401\\7.2688\end{pmatrix},\quad \mathbf{f}=\begin{pmatrix}4.4973\\5.4989\\6.4880\\11.2309\end{pmatrix}$$

Fig. 1 shows the open-loop and closed-loop receptance, where it can be seen that the first two peaks correspond to the four assigned poles and the second two peaks to the four retained poles. The height of the third peak has changed as a result of re-assigning the eigenvalues of the first two peaks but the two eigenvalues λ_5, λ_6 remain exactly as they were, $\mu_5=\lambda_5$, $\mu_6=\lambda_6$.

6. Practical continuous structures

In the case of continuous structures with, in theory, infinite numbers of vibration modes the frequency range of operation is known so that only that part of the spectrum within the frequency range needs to be controlled. Then the task of the controller may be defined as assigning the selected eigenvalues while retaining unchanged the other open-loop eigenvalues within the frequency range of operation, using a limited number of sensors and actuators and without knowledge of the order of the system (the number of degrees of freedom). By this definition it is clear that the orthogonality conditions are not available. Therefore partial pole placement by the unobservability condition is not possible. It is however possible by using the uncontrollability condition.

To illustrate this capability we now re-define the matrices $\mathbf{\Lambda}_2$ and $\mathbf{\Psi}_2$ as follows:

$$\dim(\mathbf{\Lambda}_2)=m'\times m',\quad \dim(\mathbf{\Phi}_2)=n'\times m',\quad n'\le n;\quad m'\le n-m \tag{38),(39}$$

where the individual elements are selected from the available measured modes and sensors according to,

$$\mathbf{\Lambda}_2=\mathrm{diag}(\lambda_k),\quad \mathbf{\Phi}_2=[\varphi_{i,k}],\quad k\in\{m+1\quad\ldots\quad n\},\quad i\in\{1\quad\ldots\quad n\} \tag{40),(41}$$

A particular advantage is that the modes may be selected within the range of a vibration test from an engineering structure with uncountably many modes of vibration; in theory $n=\infty$.

When the actuators are placed at the same locations as the sensors, then a sufficient condition for determining $\mathbf{b}(s)$ is that $n'>m'$, i.e. that there are more sensors than the number of retained modes. The gains, **g**, **f** may then be selected to assign the closed-loop poles $\{\mu_k\}$, $\{\mu_k^*\}$ as described by Ram and Mottershead [6].

7. Lightweight glass-fibre beam

The vibration of a 45×5 mm cross-section glass-fibre cantilever beam, 600 mm long, is considered, as shown in the diagram in Fig. 2. Attached to opposite surfaces of the beam are two pairs of multi fibre composite (MFC) patches, labelled in Fig. 2. The beam is clamped at the fixed end to a heavy rigid mass shown. The smaller pair of patches (Smart Materials M-2807-P2) shown in Fig. 3(a) are used as sensors. The larger pair of patches (Smart Materials M-8528-P1) in Fig. 3(b) are

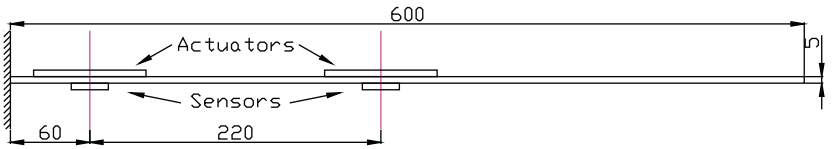

Fig. 2. Diagram of glass-fibre beam (MFC thickness increased for clarity).

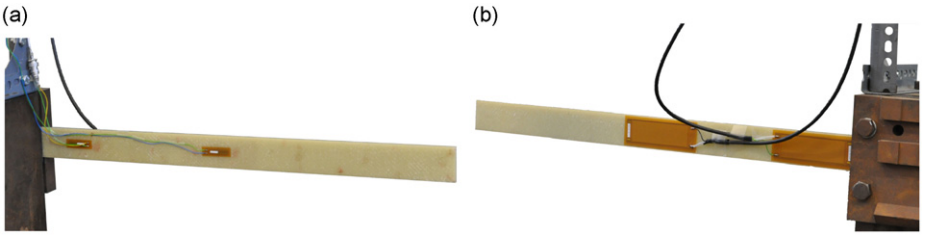

Fig. 3. MFC positions: (a) rear view, showing sensors and (b) front view, showing actuators.

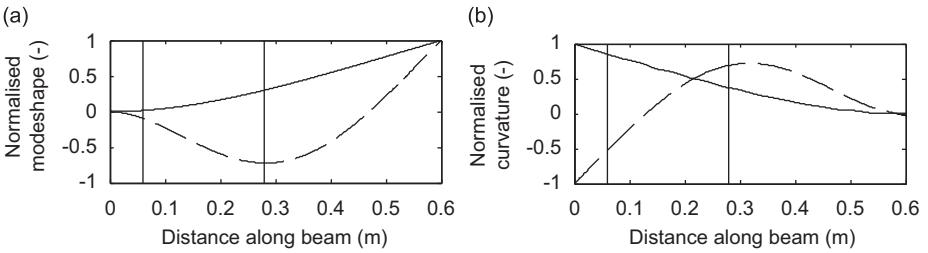

Fig. 4. Mode shapes: (a) displacement and (b) curvature. Solid—mode 1; dashed—mode 2.

used as actuators, simultaneously delivering excitation and control forces. Although the sensors and actuators are placed at the same coordinates they are not collocated in the sense of Clark et al. [20].

The input and output quantities are the voltages across the various MFC patches, the input voltage giving rise to a moment and the output voltage being proportional to curvature of the beam. It is not necessary to know either the applied moments or the resulting curvature since the receptance method is generalised to the transfer function relating the output and input voltages. The first two bending mode shapes are predicted by a finite element model and shown in Fig. 4(a) and (b), displacement and curvature, respectively.

The first actuator, at the first coordinate centred at 60 mm from the clamped end, tends to excite the first mode strongly. The second actuator, at the second coordinate located at the antinode of the curvature mode shape of the second mode (at 280 mm), excites the second mode strongly. Therefore the first and second bending modes are controllable mainly by the first and second actuators, respectively. Likewise curvature of the first and second modes are observable from the first and second sensors. The actuator/sensor positions are marked on Fig. 4.

A real time test was undertaken in dSPACE with a sampling time of 100 μs. The sensor signals were passed through a Butterworth bandpass filter with cutoff frequencies of 3 Hz and 100 Hz, and digitally differentiated using MATLAB/Simulink to enable rate and proportional feedback.

The open-loop generalised receptance $\mathbf{H}(\mathrm{i}\omega)$ between the sensor voltage/actuator voltage was obtained using random excitations of 20 V, using the H_1 estimator with 512 spectral lines in the range 0–64 Hz. A significant advantage of using the measured transfer function is that the dynamics of the actuators and sensors are included. The transfer function $\mathbf{H}(s)$ was approximated by a curve fit to the measured generalised receptance $\mathbf{H}(\mathrm{i}\omega)$ using the LMS PolyMAX method [21] so that $\mathbf{H}(s)$ is defined by a pole-residue model.

7.1. Partial pole placement of the beam

Two example cases of pole placement are presented for the beam structure, altering the poles of each mode in turn while the other mode is kept constant. The 2×2 open-loop generalised receptance $\mathbf{H}(\mathrm{i}\omega)$ was measured and PolyMAX curve fits obtained as shown in Fig. 5. Each mode was fitted globally, and agreement close to the poles and the zero in $h_{11}(\mathrm{i}\omega)$ is seen to be good.

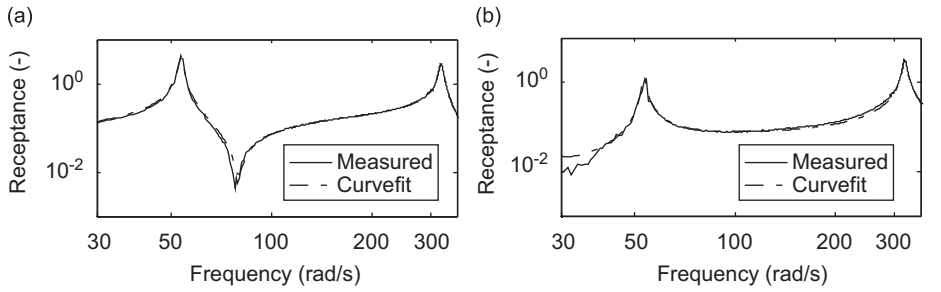

Fig. 5. Measured and curve-fitted generalised receptances: (a) $h_{11}(i\omega)$ and (b) $h_{12}(i\omega)$.

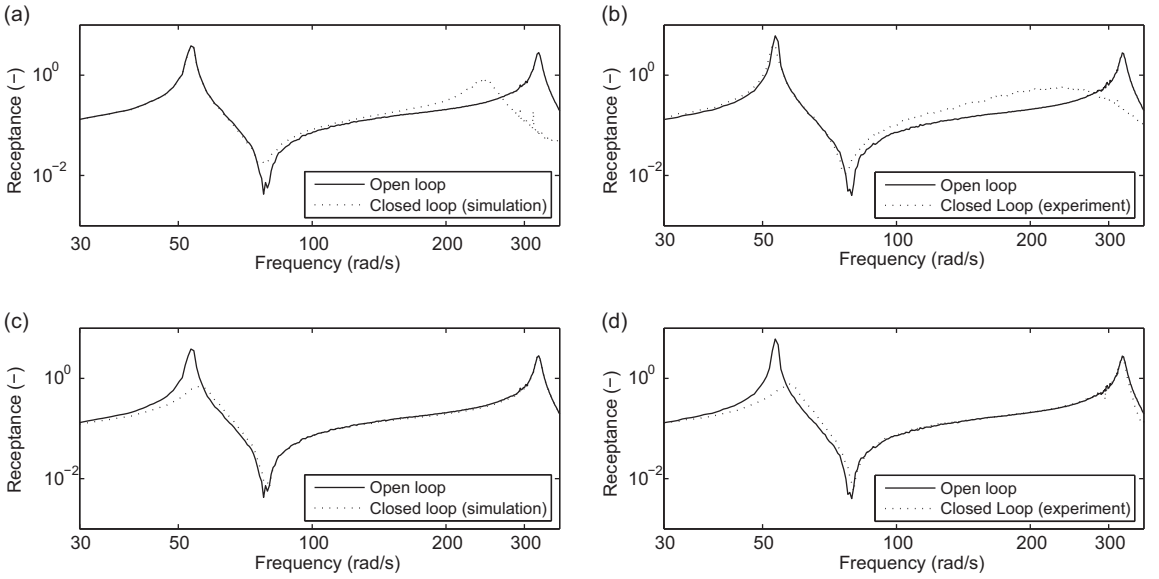

Fig. 6. Partial pole placement, $h_{11}(i\omega)$. (a), $\mathbf{b}=[-0.36\ 0.93]^T$, simulation (b) $\mathbf{b}=[-0.36\ 0.93]^T$, experiment (c) $\mathbf{b}=[0.82\ 0.56]^T$, simulation (d) $\mathbf{b}=[0.82\ 0.56]^T$, experiment.

The two curvature mode shapes of the beam, from the PolyMAX fit, were given by

$$\mathbf{\Phi}=\begin{bmatrix}1 & 1\\ 0.416 & -1.457\end{bmatrix}$$

The open-loop poles were $\lambda_{1,2}=-0.578\pm53.322i$ (first bending mode, 8.49 Hz) and $\lambda_{3,4}=-4.09\pm322.944i$ (second bending mode, 51.5 Hz). The next out of band modes were considerably higher, at 135 and 154 Hz.

7.1.1. Experiment 1: Partial pole placement of the second bending mode

To ensure a mode remains unchanged, **b** is calculated to be in the null-space of the mode shape. Thus, to avoid exciting the first mode, **b** should be in the null-space of [1 0.416], i.e. $\mathbf{b}=[-0.36\ 0.93]^T$. Using this **b** and assigning $\mu_{3,4}=-20\pm250i$, the control gains were calculated to be $\mathbf{f}=\begin{bmatrix}0.0029 & -0.0011\end{bmatrix}^T$ and $\mathbf{g}=\begin{bmatrix}-0.75 & 1.59\end{bmatrix}^T$. Figs. 6(a) and (b), for simulation and experimental implementation, respectively, shows that the first mode was unchanged (rendered uncontrollable) and the second mode appropriately reduced in frequency and damped.

7.1.2. Experiment 2: Partial pole placement of the first bending mode

To avoid exciting the second mode **b** should be in the null-space of [1 −1.457], i.e. $\mathbf{b}=[0.82\ 0.56]^T$. Using this **b** and assigning $\mu_{1,2}=-4\pm56i$, the control gains were calculated to be $\mathbf{f}=\begin{bmatrix}0.0065 & 0.0044\end{bmatrix}^T$ and $\mathbf{g}=\begin{bmatrix}-1.31 & -0.85\end{bmatrix}^T$. The first mode was increased in frequency and damped, and the second mode rendered uncontrollable, as shown in Fig. 6(c) and (d).

Fig. 6 shows excellent agreement of simulated and measured natural frequencies for both examples. The shape of the simulated and measured placed peaks in Experiment 1 differ slightly, but the increase in damping compared to the open-loop test is clearly visible. These two examples demonstrate that the receptance method may be used for partial pole placement of a generalised system, using the uncontrollability condition. Furthermore, the physical meaning of the input and output signals (in terms of moments and curvatures) is shown to be unnecessary for pole placement.

8. Sequential pole placement using multi-input state feedback

Multi-input state feedback for the assignment of eigenvalues is considered in this section. A significant advantage of the multi-input approach is that it becomes possible to select a different $\mathbf{b}(s)$ for each assigned mode. Since the control force is given by $\mathbf{b}(s)u(s)$ it is clear that each $\mathbf{b}(s)$ may be chosen readily to excite a particular mode, μ_k, while other modes j are rendered uncontrollable $\boldsymbol{\varphi}_j^{\mathrm{T}}\mathbf{b}(\lambda_j)=0$, $\lambda_j \neq \mu_k$. The multi-input state feedback equations are usually expressed in the form:

$$(\mathbf{M}s^2+\mathbf{C}s+\mathbf{K})\mathbf{x}(s)=\mathbf{B}(s)\mathbf{u}(s)+\mathbf{p}(s), \quad \mathbf{u}(s)=(\mathbf{G}+s\mathbf{F})^{\mathrm{T}}\mathbf{x}(s) \tag{42}$$

where

$$\mathbf{B}(s)=\begin{bmatrix}\boldsymbol{\beta}_1(s) & \boldsymbol{\beta}_2(s) & \cdots & \boldsymbol{\beta}_n(s)\end{bmatrix}, \quad \mathbf{G}=\begin{bmatrix}\mathbf{g}_1 & \mathbf{g}_2 & \cdots & \mathbf{g}_n\end{bmatrix}, \quad \mathbf{F}=\begin{bmatrix}\mathbf{f}_1 & \mathbf{f}_2 & \cdots & \mathbf{f}_n\end{bmatrix}$$

or,

$$(\mathbf{M}s^2+\mathbf{C}s+\mathbf{K})\mathbf{x}(s)=\left(\sum_{i=1}^{n}\boldsymbol{\beta}_i(\mathbf{g}_i+s\mathbf{f}_i)^{\mathrm{T}}\mathbf{x}(s)\right)+\mathbf{p}(s) \tag{43}$$

so that apart from the disturbance $\mathbf{p}(s)$, the right-hand side of Eq. (43) represents a series of single-input control terms, which may be applied sequentially [12]. To explain briefly here, we consider the simple case of a two-input system. Step 1: The first pair of eigenvalues are assigned by single-input state feedback with the first control vector $\boldsymbol{\beta}_1(s)$ chosen so that it easily excites the first mode pair. Step 2: $\boldsymbol{\beta}_2(s)$ is chosen so that $\boldsymbol{\psi}_1^{\mathrm{T}}\boldsymbol{\beta}_2=0$, $\boldsymbol{\psi}_2^{\mathrm{T}}\boldsymbol{\beta}_2=0$ ($\boldsymbol{\psi}_2=\boldsymbol{\psi}_1^*$) and the second mode pair are easily excited, where $\boldsymbol{\psi}_1$, $\boldsymbol{\psi}_2$ denote the left eigenvectors of the first pair of closed-loop eigenvalues already assigned in Step 1. Since the first mode pair is uncontrollable by the second input, the first pair of closed-loop eigenvalues remains unchanged.

The second pair of eigenvalues are assigned using the Sherman–Morrison–Woodbury formula, an extension of the Sherman–Morrison formula used in Section 2,

$$\overline{\mathbf{H}}(s)=\mathbf{H}(s)-\mathbf{H}(s)\mathbf{B}(s)(\mathbf{I}+(\mathbf{G}+s\mathbf{F})^{\mathrm{T}}\mathbf{H}(s)\mathbf{B}(s))^{-1}(\mathbf{G}+s\mathbf{F})^{\mathrm{T}}\mathbf{H}(s) \tag{44}$$

where $\mathbf{g}_1$, $\mathbf{f}_1$, $\boldsymbol{\beta}_1(s)$ are fixed from the first assignment step and $\boldsymbol{\psi}_1^{\mathrm{T}}\boldsymbol{\beta}_2=0$, $\boldsymbol{\psi}_2^{\mathrm{T}}\boldsymbol{\beta}_2=0$. The characteristic equations for assigning the second pair of eigenvalues are given by

$$\det(\mathbf{I}+(\mathbf{G}+\mu_{3,4}\mathbf{F})^{\mathrm{T}}\mathbf{H}(\mu_{3,4})\mathbf{B}(\mu_{3,4}))=0, \quad \mu_4=\mu_3^* \tag{45}$$

Subsequently a third pair of eigenvalues may be assigned when $\boldsymbol{\beta}_3$ is chosen so that $\begin{bmatrix}\boldsymbol{\psi}_1^{\mathrm{T}}\\ \boldsymbol{\psi}_3^{\mathrm{T}}\end{bmatrix}\boldsymbol{\beta}_3=0$, $\begin{bmatrix}\boldsymbol{\psi}_2^{\mathrm{T}}\\ \boldsymbol{\psi}_4^{\mathrm{T}}\end{bmatrix}\boldsymbol{\beta}_3=0$, which may be achieved using Eqs. (34)–(37) but substituting the closed-loop left eigenvectors $\boldsymbol{\Psi}=\begin{bmatrix}\boldsymbol{\psi}_1 & \boldsymbol{\psi}_3\end{bmatrix}$ for the open-loop eigenvectors $\boldsymbol{\Phi}_2$. A full derivation of the sequential pole placement procedure using the Sherman–Morrison–Woodbury formula is described in [12]. In practical lightly damped metallic structures the closed-loop right and left eigenvectors change very little from the open-loop eigenvectors—advantage is taken of this observation in the experiments described in the following section.

9. Heavy modular test structure

Two configurations of a modular test structure are considered for active vibration control, as shown in Fig. 7. The structure consists of up to six box-section steel beams of 3 mm wall-thickness and up to six block-masses. The principal dimensions are given in Fig. 8. The two main (vertical) beams have cross-sections of 75×50 mm, and the four arms (horizontal) have cross-sections of 50×25 mm. Each of the two central block-masses is 120 mm deep, and each of the four block-masses on each arm is 95 mm deep. The structure is attached at the root to a large suspended mass. The first set of tests is upon the 'T' configuration shown in Fig. 7(a), where the two upper arms and their block-masses have been removed, representing a physically symmetric system. The second set of tests is upon the 'H' configuration shown in Fig. 7(b), also representing a physically symmetric system.

Up to four Data Physics IV40 inertial shakers, simultaneously supplying the excitation and control forces, were attached to heavy rigid masses at their bases and connected to the test structure via stingers. Kistler type 8636C50 sensors at the arm-tip masses were used to measure the acceleration signals, which were passed through a Butterworth bandpass filter with cutoff frequencies of 25 and 250 Hz. The signals were digitally integrated twice using MATLAB/Simulink, thereby enabling both velocity and displacement feedback. In both configurations, coordinates 1 and 2 are the z-direction displacements at the accelerometer locations on the lower arm block-masses. In the 'H' configuration, coordinates 3 and 4

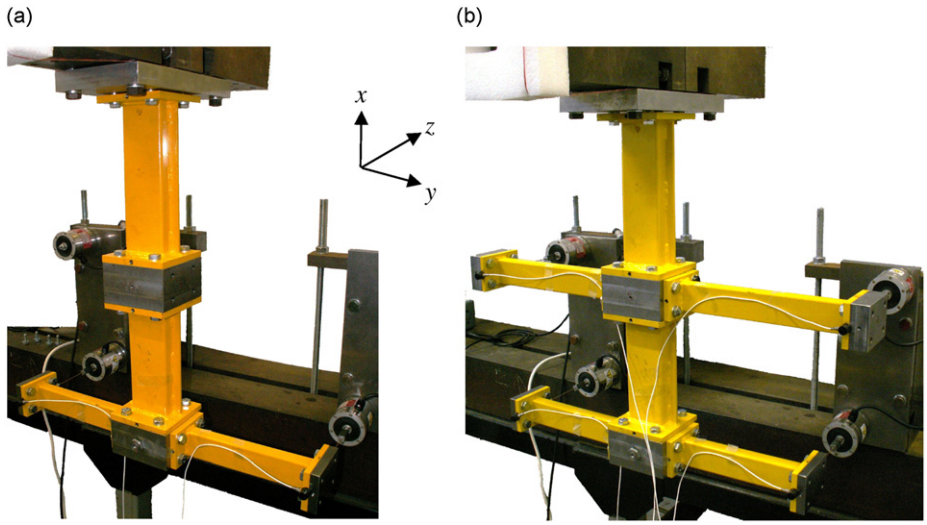

Fig. 7. Modular test structure for active vibration control: (a) 'T' configuration and (b) 'H' configuration.

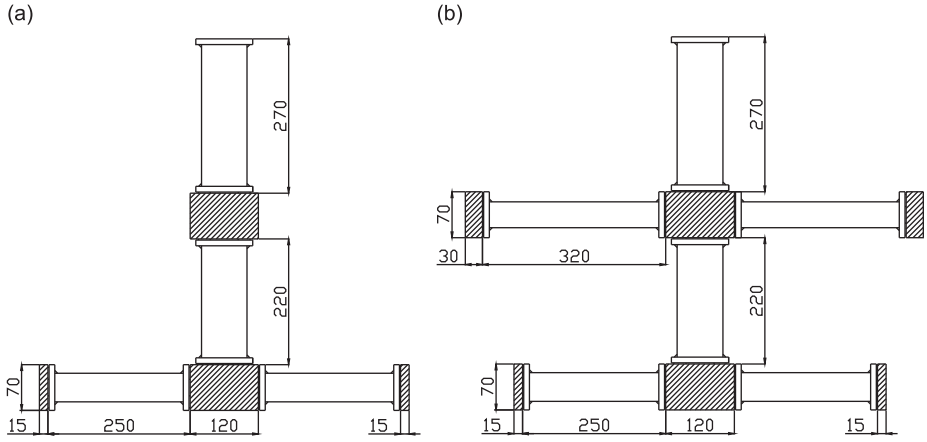

Fig. 8. Test structure configurations: (a) 'T' and (b) 'H'.

are the z-direction displacements at the accelerometer locations on the upper arms. As in the previous section the sensors and actuators are not collocated in the mathematical sense [20], although they are of course placed at the same locations physically.

The open-loop transfer function between the acceleration/input voltage was obtained using random excitations of 0.1 V, using the H_1 estimator with 2048 spectral lines in the range 0–256 Hz. The open-loop receptance, generalised here to mean displacement/input voltage, was obtained by dividing the acceleration/input voltage by $-\omega^2$. As with the glass-fibre beam experiment the measured receptance includes the dynamics of the actuators and sensors.

9.1. *Partial pole placement for the 'T' configuration*

Three example cases of pole placement are presented for this 'T' configuration, to alter the natural frequencies and damping of the modes. Open-loop tests were undertaken to obtain the full 2×2 receptance matrix $\mathbf{H}(i\omega)$, plotted in Fig. 9.

The first natural frequency (at 54 Hz, 339 rad/s) represents the first bending mode of the 'T' in the z direction. The second natural frequency (at 80 Hz, 503 rad/s) is the first torsional mode of the arms about the x-axis. The third natural frequency (at 167 Hz, 1050 rad/s) is the second bending mode of the arms in the z direction.

Fig. 9 shows the good agreement between measured and fitted receptances for $h_{11}(i\omega)$ and $h_{12}(i\omega)$. Due to the geometric symmetry of the test structure, $h_{11}(i\omega)$ and $h_{22}(i\omega)$ are almost exactly alike; $h_{12}(i\omega)$ and $h_{21}(i\omega)$ are also similar due to reciprocity.

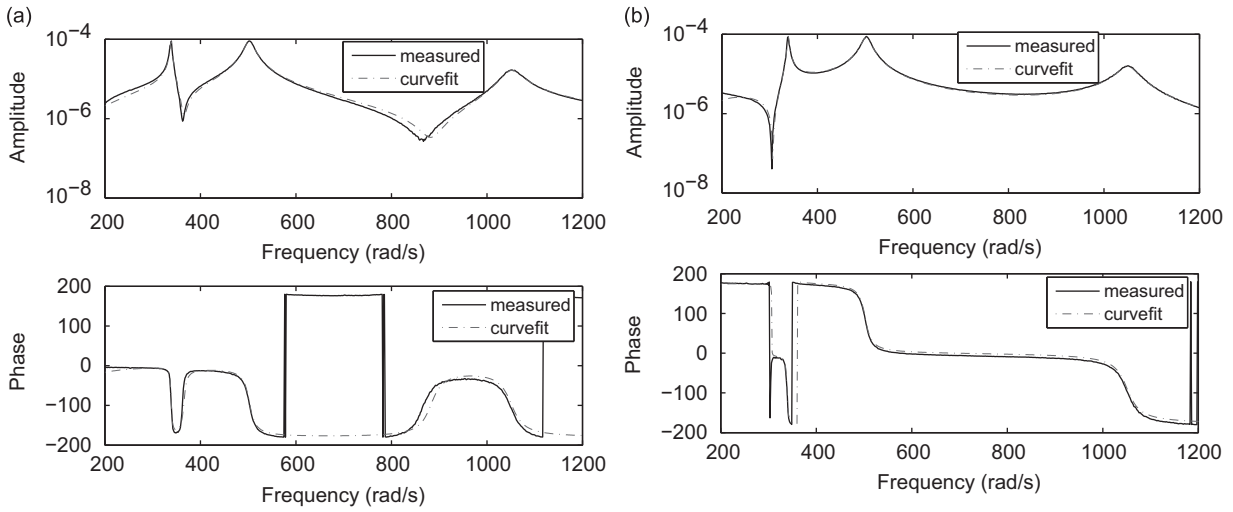

Fig. 9. Measured and curve-fitted receptances: (a) $h_{11}(i\omega)$ and (b) $h_{12}(i\omega)$.

The open-loop poles were found from the fitted transfer function as

$$\lambda_{1,2} = -2.0 \pm 339i$$
$$\lambda_{3,4} = -8.7 \pm 503i$$
$$\lambda_{5,6} = -20.0 \pm 1050i$$

9.1.1. Experiment 1: Partial pole placement of the bending mode

In this experiment, partial pole placement theory was applied to assign the first pair of poles to $\mu_{1,2} = -8 \pm 350i$, while rendering the second pair unchanged. The control distribution vector was chosen to be $\mathbf{b} = [1 \quad 1]^T$, which is in the null-space of the eigenvector of the second mode. The single-input state-feedback introduced by Ram and Mottershead [6] was used to obtain the control gains,

$$\mathbf{g} = \begin{bmatrix} 19000 \\ 19000 \end{bmatrix}, \quad \mathbf{f} = \begin{bmatrix} 34 \\ 34 \end{bmatrix}$$

Note that the identical terms in each control vector are due to the physical symmetry of the structure. The closed-loop receptance h_{11} was simulated using the control gains above and the measured open-loop receptance, and is plotted in Fig. 10(a). As expected, the poles are assigned at the prescribed values. A real time test was undertaken in dSPACE with a sampling time of 100 μs. The measured closed-loop receptance h_{11} is plotted in Fig. 10(b). A comparison of the two plots shows very good agreement between the simulated and measured closed-loop behaviour.

9.1.2. Experiment 2: Partial pole placement of the torsional mode

In this experiment, the second pair of poles was assigned to $\mu_{3,4} = -60 \pm 535i$. The control gains were found to be

$$\mathbf{b} = \begin{bmatrix} 1 \\ -1 \end{bmatrix}, \quad \mathbf{g} = \begin{bmatrix} 10\,862 \\ -10\,862 \end{bmatrix}, \quad \mathbf{f} = \begin{bmatrix} 30 \\ -30 \end{bmatrix}$$

Fig. 11(a) and (b) again show very good agreement between the simulated and experimental results.

9.1.3. Experiment 3: Simultaneous assignment of the two modes using multi-input state feedback

In this experiment, two pairs of poles were assigned using multi-input state feedback described in Section 8. In the first step, the bending mode was assigned and the control gains $\mathbf{f}_1$ and $\mathbf{g}_1$ were obtained. In the second step, the torsional mode was assigned while the assigned bending mode was unchanged. The prescribed poles and the control gains are shown for two different cases.

Case 1:

$$\mu_{1,2} = -13 \pm 350i$$
$$\mu_{3,4} = -30 \pm 610i$$

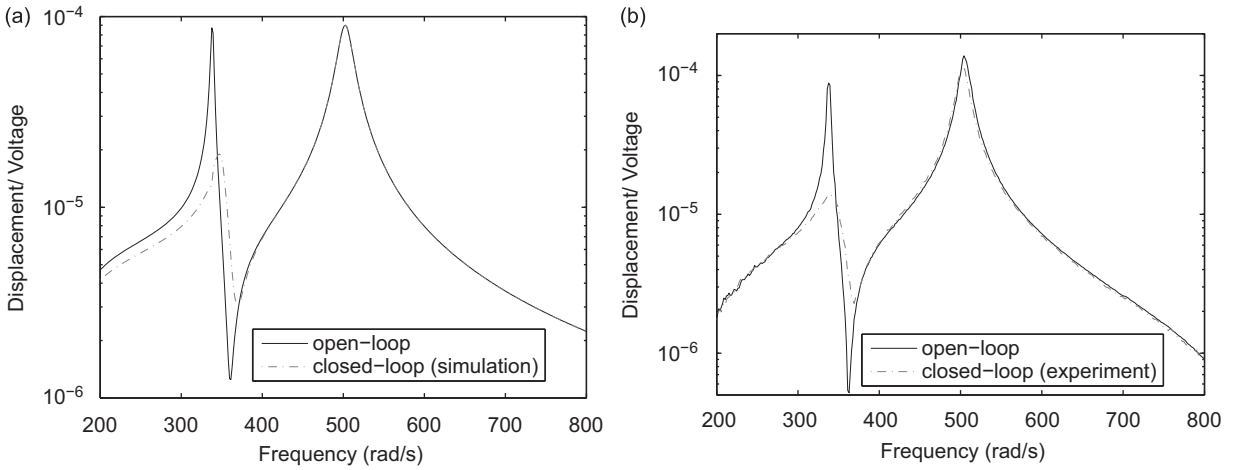

Fig. 10. Partial pole placement of the bending mode, h_{11}: (a) simulation and (b) experiment.

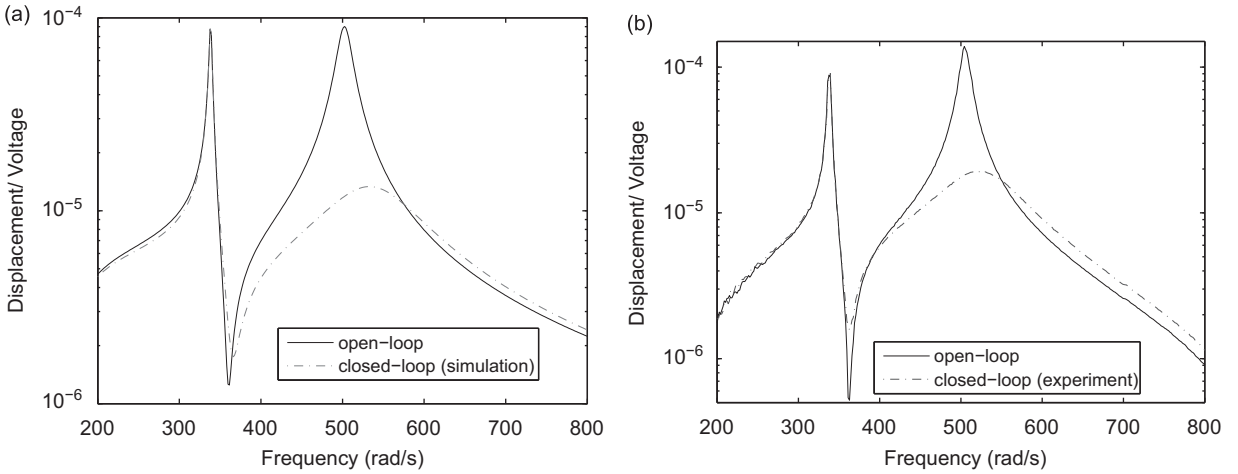

Fig. 11. Partial pole placement of the torsional mode, h_{11}: (a) simulation and (b) experiment.

$$\mathbf{B}=\begin{bmatrix}1 & 1\\ 1 & -1\end{bmatrix},\quad \mathbf{G}=\begin{bmatrix}17900 & 34000\\ 17900 & -34000\end{bmatrix},\quad \mathbf{F}=\begin{bmatrix}61 & 13\\ 61 & -13\end{bmatrix}$$

Case 2:

$$\mu_{1,2}=-11\pm 352\mathrm{i}$$
$$\mu_{3,4}=-40\pm 680\mathrm{i}$$
$$\mathbf{B}=\begin{bmatrix}1 & 1\\ 1 & -1\end{bmatrix},\quad \mathbf{G}=\begin{bmatrix}22\,000 & 60\,000\\ 22\,000 & -60\,000\end{bmatrix},\quad \mathbf{F}=\begin{bmatrix}52 & 20\\ 52 & -20\end{bmatrix}$$

Fig. 12 shows the full range of measurements taken, where two outlying modes can also be seen: a rigid body mode at 10 Hz in the *y* direction (labelled mode 1) and the second bending mode of the 'T' in the *z* direction (mode 4). The system is stable over the range 0–1600 rad/s. Note that due to the similarity of the mode shapes of modes 2 and 4 in the simplified 2DOF model used, control on one of these modes will affect the other. The addition of an actuator at the centre of the 'T' would allow the two modes to be controlled independently. Results obtained from simulation and experiments are plotted in Fig. 13. The results are in very good agreement, and the poles are assigned to prescribed values.

9.2. Partial pole placement for the 'H' configuration

A second configuration was considered with all the arms attached to the main beams, as in Fig. 7(b). Four inertial actuators (Data Physics IV40) and four sensors (Kistler accelerometer type 8636C50) were used to assign four pairs of

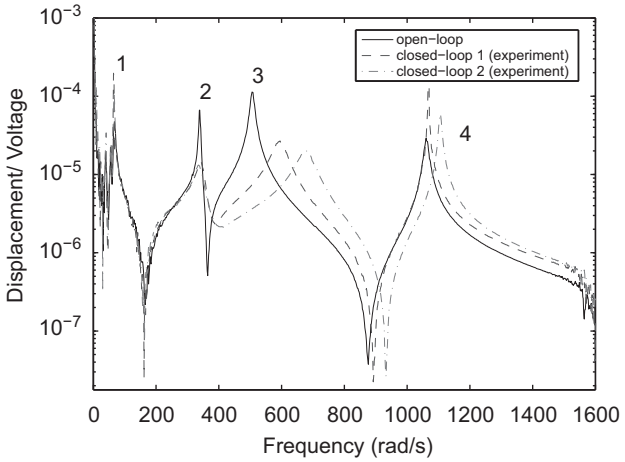

Fig. 12. Partial pole placement of the two modes, h_{11}.

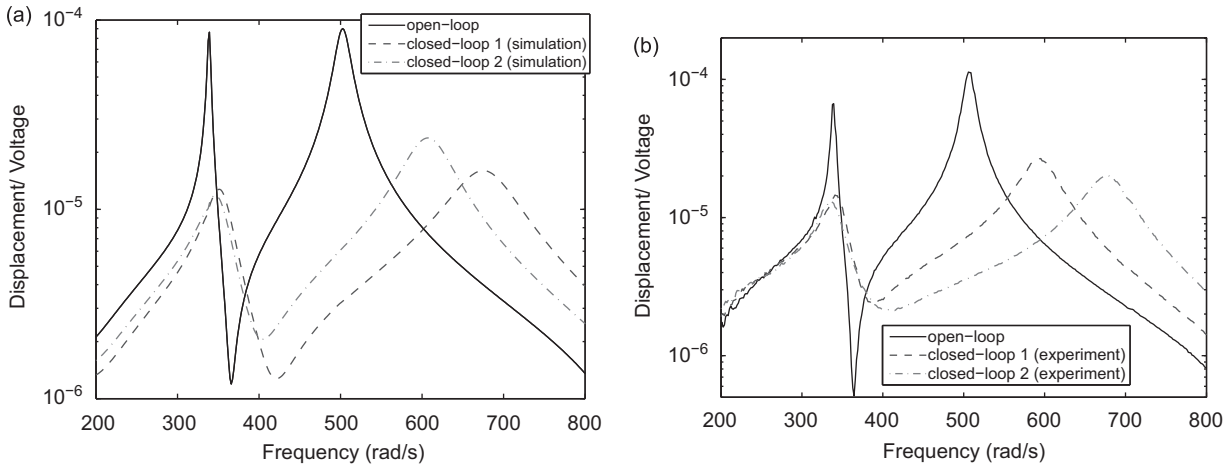

Fig. 13. Partial pole placement of the two modes, h_{11}: (a) simulation and (b) experiment.

complex conjugate poles corresponding to the first four flexural modes of the structure. The test setup was the same as with the 'T' configuration. The mode shapes of the first five natural frequencies of the open-loop system are shown in Fig. 14. The first mode (54 Hz, 338 rad/s) was a bending mode of the main beams. The second mode (60 Hz, 377 rad/s) was the torsional mode of the main beams, with the upper and lower arms in-phase. The third mode (86 Hz, 538 rad/s) showed the in-phase bending of the upper arms. The fourth mode (96 Hz, 603 rad/s) was the torsional mode of the main beams with the upper and lower arms out of phase. The fifth mode (167 Hz, 1050 rad/s) showed the in-phase bending of the lower arms.

The point receptance terms $h_{11}(\mathrm{i}\omega)$ and $h_{22}(\mathrm{i}\omega)$ were almost identical to $h_{33}(\mathrm{i}\omega)$ and $h_{44}(\mathrm{i}\omega)$, respectively, because of geometric symmetry of the structure, and due to reciprocity the cross-receptance terms such as $h_{12}(\mathrm{i}\omega)$ and $h_{21}(\mathrm{i}\omega)$ were found to be similar. The fitted receptances are presented for measured receptance terms $h_{11}(\mathrm{i}\omega)$, $h_{12}(\mathrm{i}\omega)$, $h_{33}(\mathrm{i}\omega)$ and $h_{34}(\mathrm{i}\omega)$ in Fig. 15, where measurements are represented by full lines and fitted curves are shown as dashed-dotted lines. There is a good agreement between the measured and the curve-fitted data.

The open-loop poles were found from the fitted transfer function as

$$\lambda_{1,2} = -1.31 \pm 338\mathrm{i}$$
$$\lambda_{3,4} = -4.08 \pm 377\mathrm{i}$$
$$\lambda_{5,6} = -4.52 \pm 538\mathrm{i}$$
$$\lambda_{7,8} = -6.16 \pm 603\mathrm{i}$$

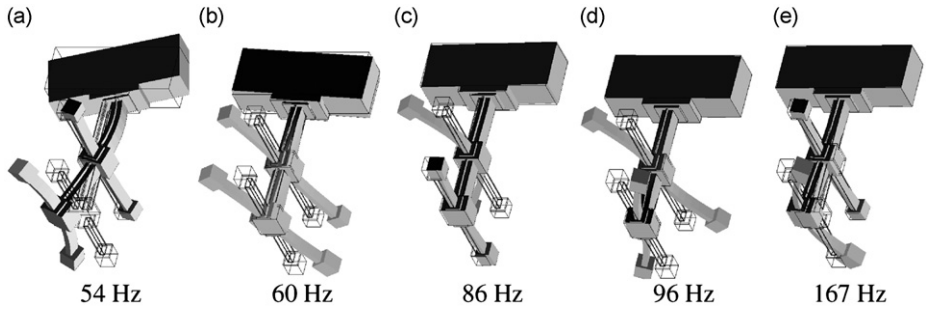

Fig. 14. 'H' test configuration mode shapes.

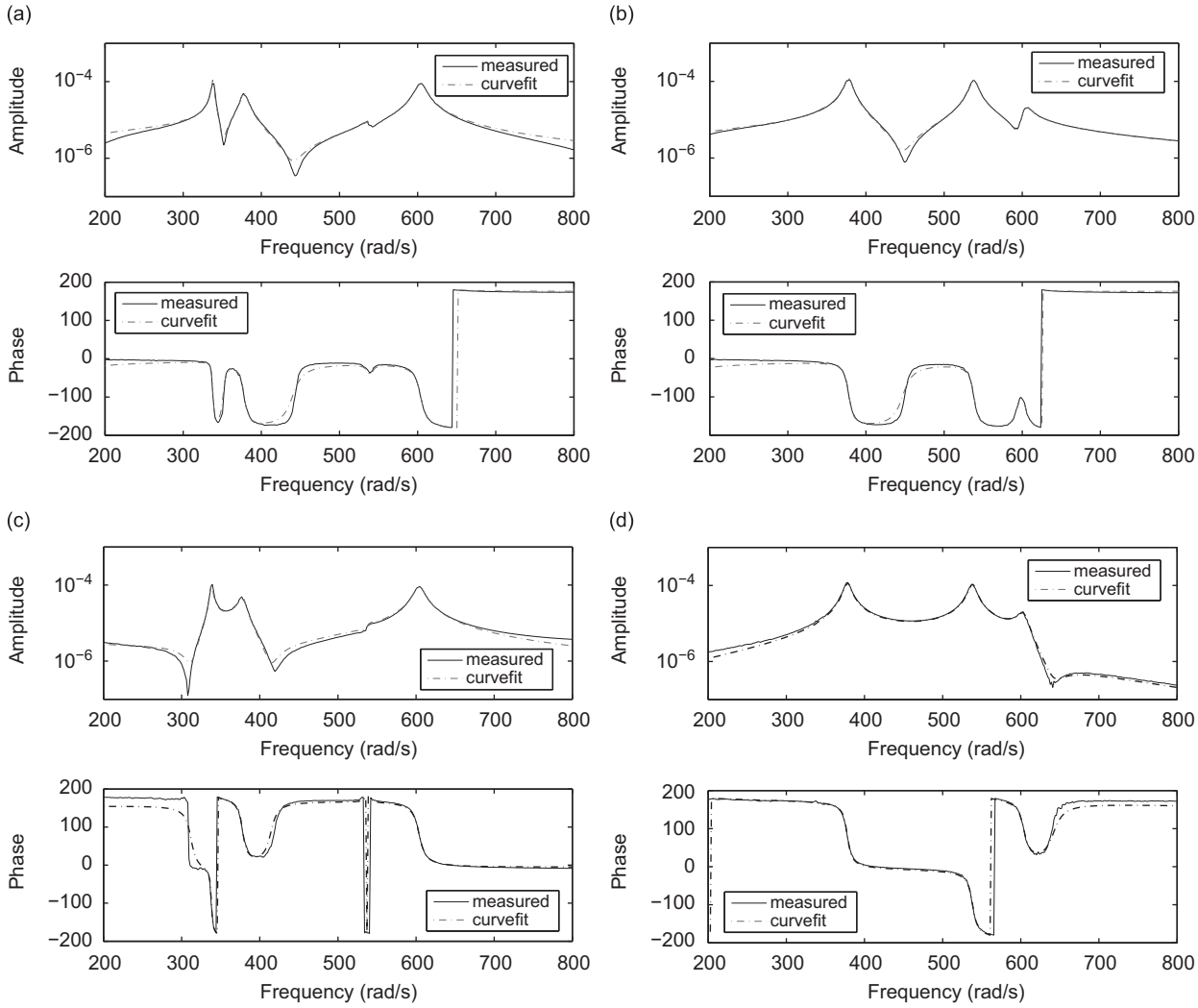

Fig. 15. Measured and curve-fitted receptances: (a) $h_{11}(i\omega)$, (b) $h_{33}(i\omega)$, (c) $h_{12}(i\omega)$ and (d) $h_{34}(i\omega)$.

9.2.1. Experiment 1: Partial pole placement of the bending modes

Poles were to be assigned at $\mu_{1,2} = -12 \pm 340i$ and $\mu_{5,6} = -30 \pm 550i$. The control force distribution $\mathbf{b} = [1 \quad 1 \quad 1 \quad 1]^T$ was chosen so that the two bending modes were excited easily while retaining the torsional modes without change. The control gains were found to be $\mathbf{g} = [5700 \quad 5700 \quad 9760 \quad 9760]^T$ and $\mathbf{f} = [57 \quad 57 \quad 32 \quad 32]^T$. Fig. 16 shows simulation and experimental displacement/input voltage for the open-loop system as the full lines and the closed-loop system as

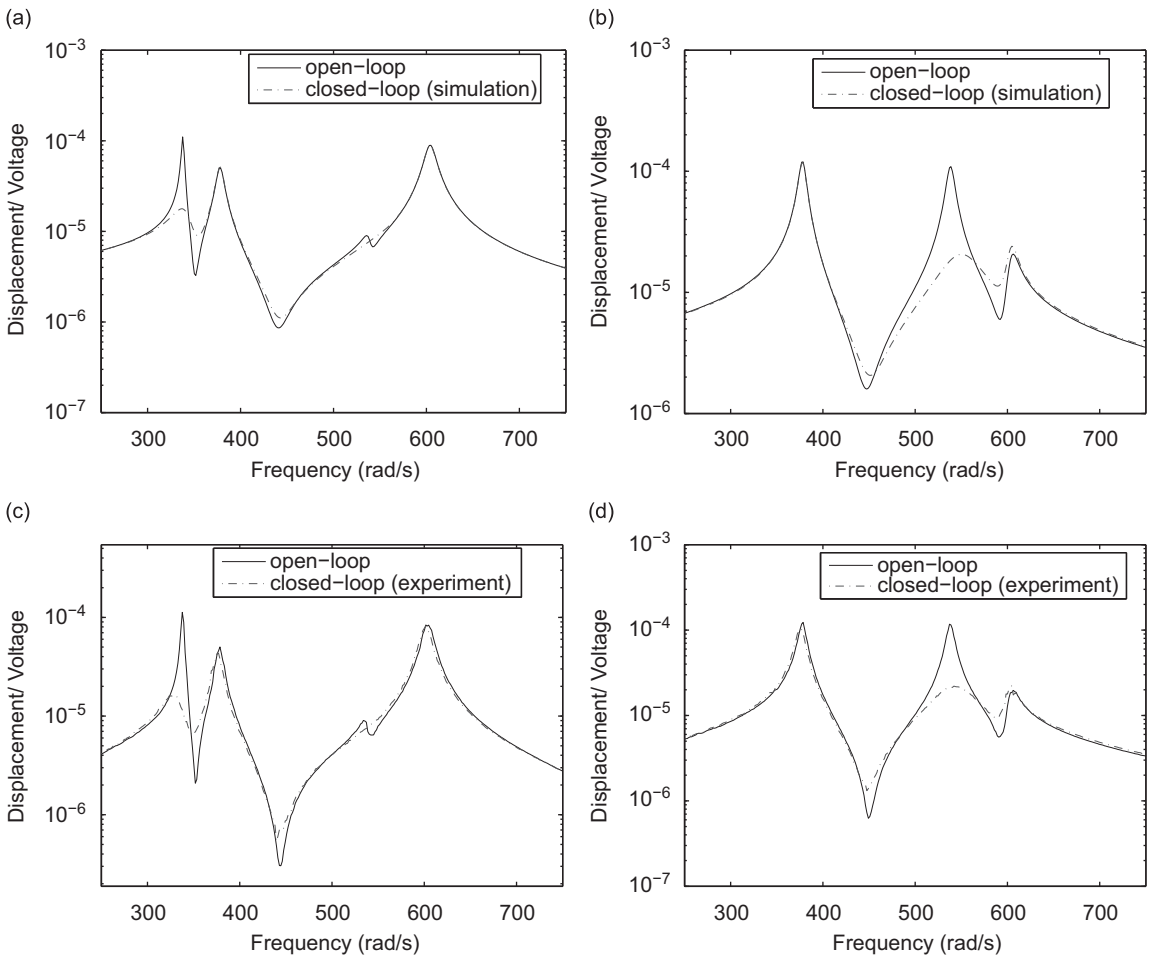

Fig. 16. Partial pole placement of the bending modes: simulation—(a) h_{11}, (b) h_{33}, experiment—(c) h_{11} and (d) h_{33}.

dashed-dotted lines for h_{11} and h_{33}. It can be seen that the two bending modes were controlled with significant increases in damping, and that the torsional modes were not affected by the control force.

9.2.2. Experiment 2: Partial pole placement of the torsional modes

Poles were to be assigned at $\mu_{3,4} = -12 \pm 410\mathrm{i}$ and $\mu_{7,8} = -65 \pm 640\mathrm{i}$. The control force distribution $\mathbf{b} = [1 \quad -1 \quad 1 \quad -1]^{\mathrm{T}}$ was chosen so that the two torsional modes were easily excited. The control gains were found to be $\mathbf{g} = [20\,000 \quad -20\,000 \quad 840 \quad -840]^{\mathrm{T}}$ and $\mathbf{f} = [-55 \quad 55 \quad 16 \quad -16]^{\mathrm{T}}$. Fig. 17 shows the simulated and measured displacement/input voltage for the open-loop system as the full lines and the closed-loop system as dashed-dotted lines, for $h_{11}$and h_{33}. Both simulated and measured results show that the torsional mode poles were assigned to the prescribed values, while the bending modes were rendered uncontrollable. The mode at 54 Hz, labelled mode 1 in Fig. 12, disappears in h_{33} and h_{44}, since the upper arms are at a node of the bending mode in Fig. 14(a). Similarly, the mode at 85 Hz (labelled mode 3) almost disappears in h_{11} and h_{22}, since the lower arms are very close to a node of the mode shape shown in Fig. 14(c).

9.2.3. Experiment 3: Simultaneous assignment of all four modes using multi-input state feedback

In this experiment two tests were carried out. In the first test, the two pairs of poles correspond to bending modes were assigned to $\mu_{1,2} = -4 \pm 342\mathrm{i}$ and $\mu_{5,6} = -12 \pm 545\mathrm{i}$ by single-input state feedback using $\mathbf{b}_1 = [1 \quad 1 \quad 1 \quad 1]^{\mathrm{T}}$ and the control gains $\mathbf{g}_1 = [4200 \quad 4200 \quad 3500 \quad 3500]^{\mathrm{T}}$ and $\mathbf{f}_1 = [15 \quad 15 \quad 10 \quad 10]^{\mathrm{T}}$ were obtained. Then the other two pairs corresponding with the torsional modes were assigned to $\mu_{3,4} = -6 \pm 435\mathrm{i}$ and $\mu_{7,8} = -25 \pm 645\mathrm{i}$ using partial pole placement. The force distribution vector was chosen as $\mathbf{b}_2 = [1 \quad -1 \quad 1 \quad -1]^{\mathrm{T}}$ so that the previously assigned poles remained unchanged. The control gains were obtained from the theory of the sequential multi-input state feedback [12]

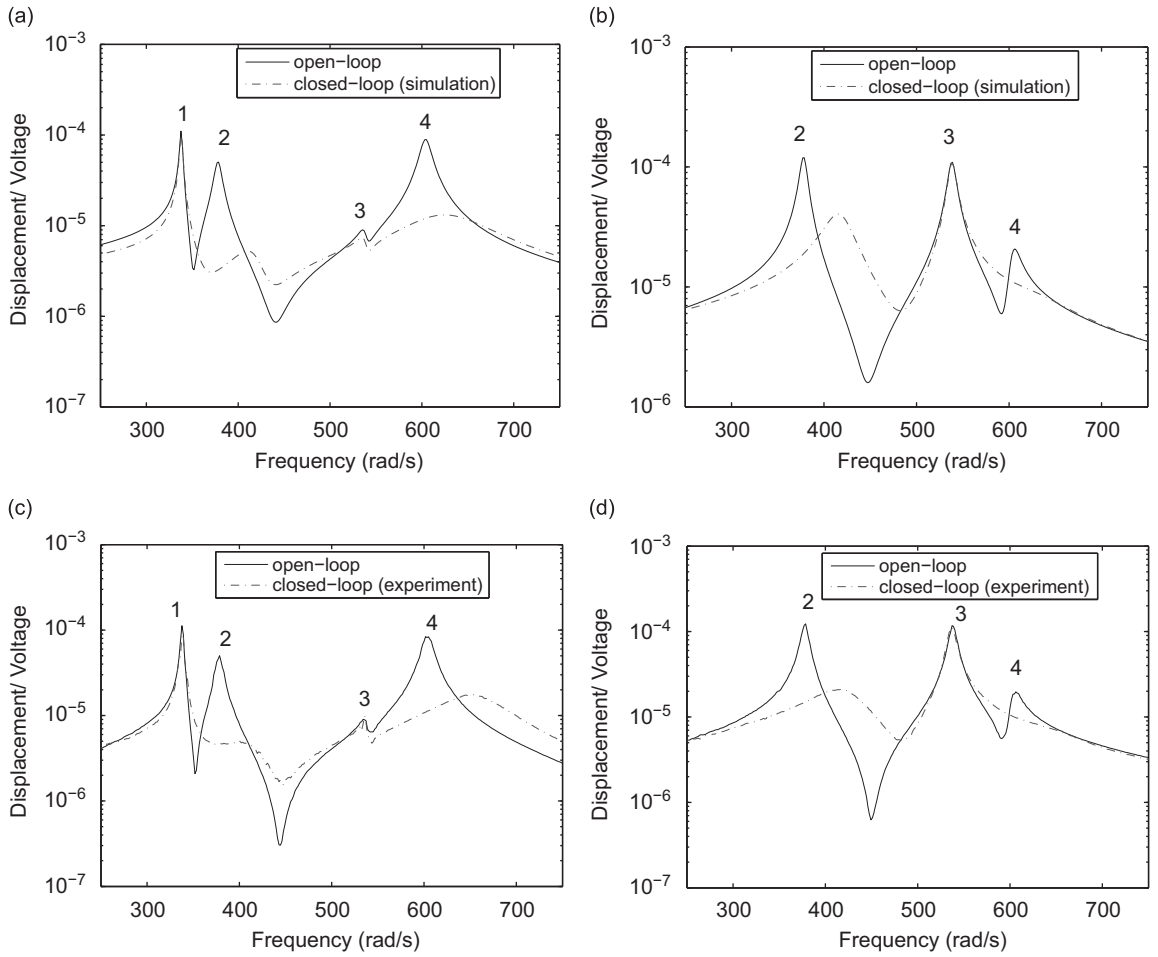

Fig. 17. Partial pole placement of the bending modes: simulation—(a) h_{11}, (b) h_{33}, experiment—(c) h_{11} and (d) h_{33}.

as $\mathbf{g}_2 = [\,24\,500 \quad -24\,500 \quad 10\,500 \quad -10\,500\,]^{\mathrm{T}}$ and $\mathbf{f}_2 = [\,20 \quad -20 \quad -3 \quad 3\,]^{\mathrm{T}}$. Therefore,

$$\mathbf{B} = \begin{bmatrix} 1 & 1 \\ 1 & -1 \\ 1 & 1 \\ 1 & -1 \end{bmatrix}, \quad \mathbf{G} = \begin{bmatrix} 4200 & 24500 \\ 4200 & -24500 \\ 3500 & 10500 \\ 3500 & -10500 \end{bmatrix} \text{ and } \mathbf{F} = \begin{bmatrix} 15 & 20 \\ 15 & -20 \\ 10 & -3 \\ 10 & 3 \end{bmatrix}$$

In the second test, the poles were assigned to

$$\mu_{1,2} = -10 \pm 340\mathrm{i}$$
$$\mu_{3,4} = -12 \pm 440\mathrm{i}$$
$$\mu_{5,6} = -20 \pm 540\mathrm{i}$$
$$\mu_{7,8} = -45 \pm 660\mathrm{i}$$

with

$$\mathbf{B} = \begin{bmatrix} 1 & 1 \\ 1 & -1 \\ 1 & 1 \\ 1 & -1 \end{bmatrix}, \quad \mathbf{G} = \begin{bmatrix} 3162 & 30\,000 \\ 3162 & -30\,000 \\ 1187 & 6000 \\ 1187 & -6000 \end{bmatrix} \text{ and } \mathbf{F} = \begin{bmatrix} 44 & 37 \\ 44 & -37 \\ 20 & -2.5 \\ 20 & 2.5 \end{bmatrix}$$

Fig. 18 shows the measured receptances in the range 0–1600 rad/s. As with the 'T' configuration, the outlying modes at approximately 10 and 167 Hz are seen. There is an unavoidable spillover effect on the mode at 167 Hz but the system remains stable over the entire range.

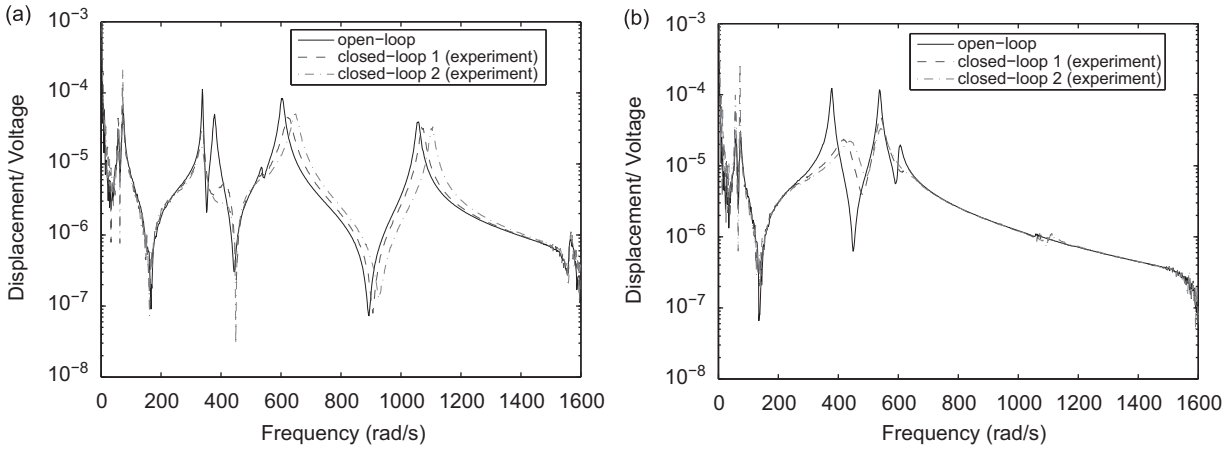

Fig. 18. Assignment of all four modes using multi-input state feedback: (a) h_{11} and (b) h_{33}.

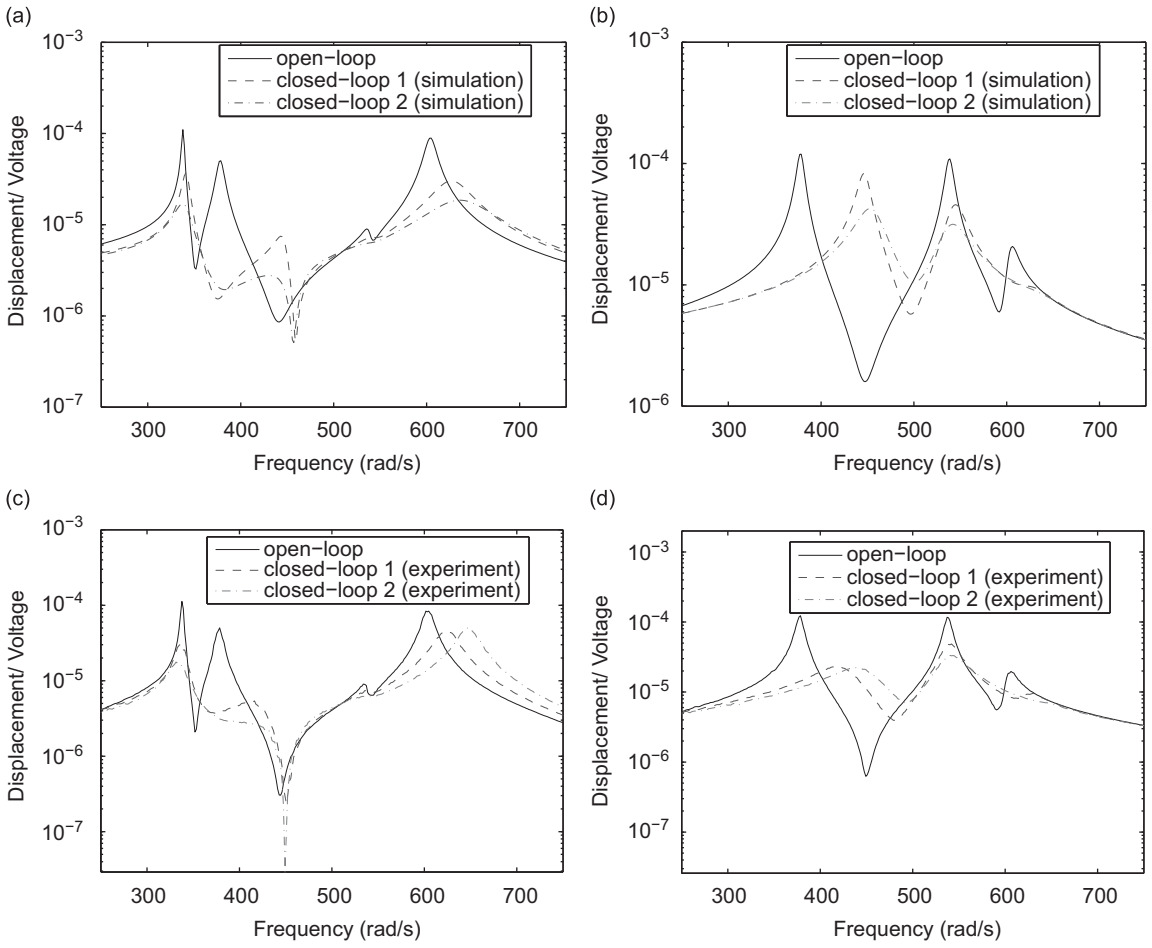

Fig. 19. Assignment of all four modes using multi-input state feedback: simulation—(a) h_{11},(b) h_{33}; experiment—(c) h_{11}, (d) h_{33}.

The simulated and experimental receptances are shown in Fig. 19. The open-loop receptance is shown using full lines and for the closed-loop system the dashed and dashed-dotted lines show the closed-loop receptances for the first and second test respectively.

10. Conclusions

In this research, the theory of the receptance method for single-input and multi-input state feedback partial pole placement were developed and demonstrated using two experimental rigs: (1) a lightweight glass-fibre beam with MFC actuators and (2) a heavy modular test structure in two configurations using electromagnetic actuators and piezoelectric accelerometers. The receptance method does not require knowledge or evaluation of the system matrices **M**, **C**, **K**, or of the actuator dynamics, which may be included in the measurement by generalisation of the receptance. Poles were assigned sequentially, the force distribution vector in each step being selected from the null-space of previously assigned modes to easily excite the next mode, thereby ensuring that previously assigned poles are uncontrollable and remain unchanged. Very good agreement between simulated and measured poles was demonstrated, both in the assigned natural frequencies and damping.

Acknowledgement

The authors wish to acknowledge the support provided by EPSRC Grant EP/F008724/1.

References

[1] J.E. Mottershead, Y.M. Ram, Inverse eigenvalue problems in vibration absorption: passive modification and active control, *Mechanical Systems and Signal Processing* 20 (1) (2006) 5–44.
[2] W.M. Wonham, On pole assignment in multi-input controllable linear systems, *IEEE Transactions on Automatic Control, AC* 12 (6) (1967) 660–665.
[3] B. Porter, R. Crossley, *Modal Control: Theory and Applications*, Taylor & Francis, London, 1972.
[4] E.K. Chu, B.N. Datta, Numerically robust pole assignment for second order systems, *International Journal of Control* 64 (4) (1996) 1113–1127.
[5] D. Del Vescovo, W. D'Ambrogio, Control of a flexible link by shaping the control loop frequency response function through optimised feedback filters, *Mechanical Systems and Signal Processing* 9 (1) (1995) 1–13.
[6] Y.M. Ram, J.E. Mottershead, Receptance method in active vibration control, *American Institute of Aeronautics and Astronautics Journal* 45 (3) (2007) 562–567.
[7] B.N. Datta, S. Elhay, Y.M. Ram, Orthogonality and partial pole assignment for the symmetric definite quadratic pencil, *Linear Algebra and its Applications* 257 (1997) 29–48.
[8] B.N. Datta D.R. Sarkissian, Multi-input partial eigenvalue assignment for the symmetric quadratic pencil, in: *Proceedings of the American Control Conference*, San Diego, California, 1999, pp. 2244–2247.
[9] J. Qian, S. Xu, Robust partial eigenvalue assignment problem for the second-order system, *Journal of Sound and Vibration* 282 (2005) 937–948.
[10] S. Brahma, B.N. Datta, An optimisation approach for minimum norm and robust partial quadratic eigenvalue assignment problems for vibrating structures, *Journal of Sound and Vibration* 324 (2009) 471–489.
[11] Z-J. Bai, B.N. Datta, J Wang, Robust and minimum norm partial quadratic eigenvalue assignment in vibrating systems: a new optimisation approach, *Mechanical Systems and Signal Processing* 24 (2010) 766–783.
[12] M.G. Tehrani, J.E. Mottershead, A.T. Shenton, Y.M. Ram, Robust pole placement in structures by the method of receptances, *Mechanical Systems and Signal Processing*, doi:10.1016/j.ymssp.2010.04.005, in press.
[13] J.E. Mottershead, M.G. Tehrani, S. James, Y.M. Ram, Active vibration suppression by pole-zero placement using measured receptances, *Journal of Sound and Vibration* 311 (3–5) (2008) 1391–1408.
[14] J.T. Xing, Y.P. Xiong, W.G. Price, A general mathematical model and analysis for integrated multi-channel vibration structure–control interaction systems, *Journal of Sound and Vibration* 320 (2009) 584–616.
[15] I. Fawzy, R.E.D. Bishop, On the dynamics of linear non-conservative systems, *Proceedings of the Royal Society of London A* 352 (1976) 25–40.
[16] J.E. Mottershead, A. Kyprianou, H. Ouyang, Structural modification, part 1: Rotational receptances, *Journal of Sound and Vibration* 284 (1–2) (2005) 249–265.
[17] G.H. Golub, C.F. Van Loan, *Matrix Computations*, Johns Hopkins University Press, Baltimore, MD, 1983.
[18] A.M.A. Hamdan, A.H. Nayfeh, Measures of modal controllability and observability for first- and second-order linear systems, AIAA, *Journal of Guidance, Control and Dynamics* 12 (3) (1989) 421–428.
[19] A. Preumont, *Vibration Control of Active Structures*, *second edition*, Kluwer Academic Publishers, Dordrecht, 2002.
[20] R.L. Clark, W.R. Saunders, G.P. Gibbs, *Adaptive Structures: Dynamics and Control*, Wiley Interscience, New York, 1998, p. 205.
[21] B. Peeters, G. Lowet, H. Van der Auweraer, J. Leuridan, A new procedure for modal parameter estimation, *Journal of Sound and Vibration* 38 (1) (2004) 24–29.